# Spinel-based Coatings for Metal Supported Solid Oxide Fuel Cells

Elena Stefan[1,#], Dragos Neagu[1], Peter Blennow Tullmar[2,3], Åsa Helen Persson[3], Bhaskar R. Sudireddy[3], David Miller[1], Ming Chen[3] and John Irvine[1*]

1 University of St Andrews, School of Chemistry,KY16 9ST, St Andrews, United Kingdom

*Corresponding author Tel.: +44(0)1334 463844, Email: jtsi@st-andrews.ac.uk

2 TOPSOE FUEL CELL A/S, Nymøllevej 66, DK – 2800, Kgs. Lyngby

3 Technical University of Denmark, Department of Energy Conversion and Storage, Frederiksborgvej 399,P.O. Box 49, Bygning 778, 4000 Roskilde

# Current address: University of Oslo, Department of Chemistry, FERMiO, Gaustadalléen 21, NO-0349 Oslo, Norway

Graphical abstract

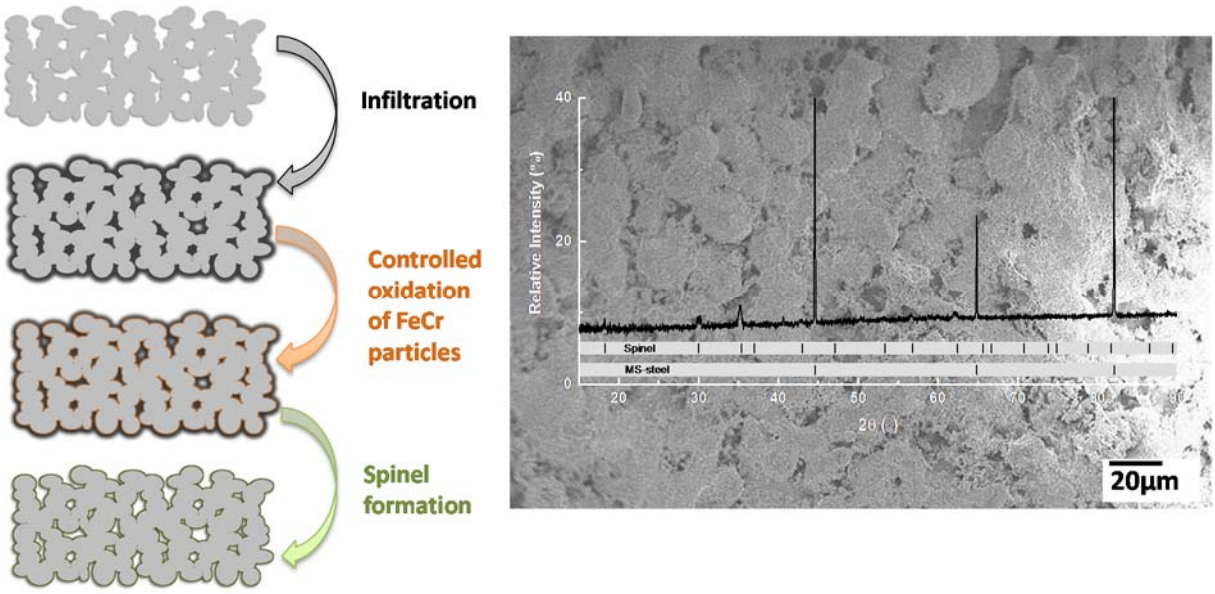

Highlights

- A successful method of solution infiltration is used for coating porous metals.
- Continuous spinel coatings were successfully prepared on porous metal scaffolds.
- Traces of Si favoured infiltration of aqueous solutions and forming spinel coatings.

**Abstract**

Metal supports and metal supported half cells developed at DTU are used for the study of a solution infiltration approach to form protective coatings on porous metal scaffolds. The metal particles in the anode layer, and sometimes even in the support may undergo oxidation in realistic operating conditions leading to severe cell degradation. Here, a controlled oxidation of the porous metal substrate and infiltration of Mn and/ or Ce nitrate solutions are applied for in situ formation of protective coatings. Our approach consists of scavenging the FeCr oxides formed during the controlled oxidation into a continuous and well adhered coating. The effectiveness of coatings is the result of composition and structure, but also of the microstructure and surface characteristics of the metal scaffolds.

Keywords: coatings; porous metal supports; solution infiltration; spinels;

# 1 Introduction

There is a strong trend in the Solid Oxide Fuel Cells (SOFCs) technology towards metal-supported SOFCs. This offers cost effective scale-up due to the anticipated lower material costs, increased tolerance to mechanical and thermal stresses and lower operational temperatures.[1,2] Some recent research has been focused on a new cell design for metal–supported SOFCs (MS-SOFCs) based on a

multi-layered structure obtainable by cost effective materials processing techniques such as tape casting, lamination, co-sintering and infiltration.[1–6] In this design, illustrated in Figure 1, the cell has a layered structure supported by a porous and highly electronically conducting FeCr-steel backbone. The anode layer consists of FeCr steel-scandium doped yttrium stabilised zirconia (ScYSZ) cermet infiltrated with $CeO_2$ and Ni.[3,7] However, in realistic operating conditions (e.g. high fuel utilisation), the corrosion resistance of the anode layer and sometimes of the metal support also are limited which raises the problem of corrosion protection for the FeCr particles, for achieving long term stability. Therefore, research efforts have been directed towards improving the corrosion resistance of metal particles in MS-SOFCs, by developing coatings[7–12] and/or new cermet materials.[13] Reasonable results were reported for nano-structured coatings of cerium doped gadolinium oxide (CGO) and Ni-CGO obtained via infiltration, with notable improvements of the corrosion resistance for the metallic components in the MS-SOFCs while maintaining high electrochemical performance.[1,2,14] Also, certain spinels, such as manganese cobaltites, have been shown previously to be quite effective at reducing $Cr_2O_3$ sub-scale formation, and blocking Cr migration when employed as dense protective coatings.[15–18]

In this study we describe the preparation and structure of several coatings obtained by infiltration-assisted scavenging of chromium and iron oxides into Cr-rich spinel layers. A Cr-rich spinel coating is expected to decrease the formation of Cr oxide scales for two reasons: the spinel would be present at the metal/oxide interface and thus lower the cation diffusion concentration-based driving force; and also Cr-spinels do not possess good oxide ion conduction to provide an oxide ion flux for further oxidation. Our approach consists of forming the spinels in-situ where oxide scales are already present on the FeCr steel support or generated specifically for this purpose in a controlled manner. Also, it is worth noting that previously we studied a range of related spinels and found they display sufficient levels of performance and stability to be used as electrode support materials.[19–22]

# 2 Experimental

For the preparation of nitrate solutions or emulsions used during the infiltration procedure, $Mn(NO_3)_2{\cdot}4H_2O$ (Alfa Aesar, 99.98%) and $Ce(NO_3)_3{\bullet}6H_2O$ (Aldrich, 99%) were employed. The resultant solutions were then infiltrated into the porous steel substrates using a pipette.

The metal supports, half cells and cermet symmetrical cells, based on 22 wt. %Cr ferritic alloy (Fe78Cr22) and ScSZ for the cermet and electrolyte layers, were prepared at as described previously by Blennow et al.[3]

The phase composition of samples after the final treatment step in reducing conditions was investigated by XRD. XRD patterns were collected for on a PANalytical Empyrean Diffractometer operated in reflection mode.

The microstructure and chemical composition of the samples (analysed with XEDS) was investigated using either a JEOL JSM-6700 or a Zeiss Crossbeam 1540XB scanning electron microscopes (SEM), both equipped with a field emission gun (FEG) at University of St Andrews (USTAN) and Technical University of Denmark (DTU), and on a JEOL JEM-2011 transmission electron microscopes (TEM) at USTAN. For this, the samples were initially embedded in resin, cut and polished, to obtain a cross-section view. The samples were then coated with a thin layer of carbon or gold to avoid charging in the electron microscope. Corrosion tests were performed at DTU on spinel coated MS and spinel coated half-cell samples for 500 h at 850 and 650 °C, in an atmosphere consisting of $Ar/H_2O/H_2$, where $pH_2O/pH_2=9$ to simulated outlet anode gas at 90% fuel utilization.

# 3 Results

## 3.1 *Coating formation procedure*

The approach employed in this study for the formation of the coatings on the steel particles is schematically illustrated in Figure 2 and discussed next. In the first step, solutions or emulsions of manganese nitrate (and/or with cerium nitrate) were infiltrated into porous metal substrates. The structures were then calcined in air at moderate temperatures, first at 350 °C and then at 600 °C, in order to decompose the nitrates into corresponding oxides and also produce a thin layer of iron and chromium oxides on the surface of metal particles. Finally, the coated porous substrates were fired at 900 °C in 5%$H_2$/Ar in order to react the $MnO_x$ and $(Fe,Cr)O_x$ phases produced in the previous steps into a spinel phase, $MnFe_xCr_{2-x}O_4$ ($x \geq 0$). It should be noted that a reducing environment (e.g. bottle dry 5%$H_2$/Ar) is necessary for this step to prevent further oxidation of the metal particles during spinel phase formation. The most stable and relatively easy to obtain in situ is $MnCr_2O_4$, since it is stable for lower $pO_2$ than $MnFe_xCr_{2-x}O_4$. According to the calculated phase diagram for Mn-Fe-Cr-$O_2$ system in the conditions employed here (900 °C and $pO_2 \sim 10^{-20}$ atm, see Figure 3 a), a spinel phase ($MnFe_xCr_{2-x}O_4$, but most likely $MnCr_2O_4$) is expected to form, possibly alongside an iron metal phase. The calculated phase diagram for Cr-Mn-$O_2$ system at 1000 °C for a wide range of $pO_2$ values (Figure 3 b), indicates that $MnCr_2O_4$ is stable and the solubility of $Cr_2O_3$ into spinel phase increases for low $pO_2$ values ($\leq 10^{-18}$ atm), which is useful for the desired application of the *in-situ* formed spinel.

Infiltration of cerium nitrate separately or in combination with manganese nitrate was investigated for a better insight of the systems and possible interactions with the oxide scale since a spinel coating would be followed by the infiltration of a Ni-CGO catalytically active phase in the anode layer of the MS-SOFC.

For improved understanding and tailoring of the *in-situ* spinel coating procedure, calculated phase diagrams[23,24] were considered (Figure 3 c, d). The calculated phase diagram at 800 °C for Ce-Cr-$O_2$ system indicates that $CeO_2$, $CeCrO_3$ and $Cr_2O_3$ are stable at $pO_2$ values between $10^{-13}$ and $10^{-18}$ atm.

For a higher temperature, 1000 °C $CeO_2$, $CeCrO_3$ and $Cr_2O_3$ are stable between $10^{-11}$ and $10^{-13}$ atm and for lower $pO_2$ values, a reduced Ce oxide, $CeCrO_3$ and $Cr_2O_3$ are stable.

## 3.2 Types of substrates

Various representative metal substrates including porous metal supports and metal supported half cells were prepared and analysed here in order to explore the formation and characteristics of the coating in different scenarios encountered in the typical MS SOFC cell architecture (see, for example, Figure 1). Porous metal supports (MS) have ~200 µm thickness and consist of coarse FeCr alloy particles. Two types porous metal supports were tested, one containing traces of surface Si as a result of furnace cross-contamination and the other clean, in order to compare the effect of surface quality on the formation of the coatings. Metal supported half cells (MSHC) consist of a ~200 µm thick FeCr porous layer, a ~30 µm thin ScYSZ/FeCr porous cermet anode functional layer and a dense ~15 µm thin ScSZ electrolyte layer.

These substrates displayed distinct behaviour during the infiltration procedure. Si-contaminated porous metal supports also displayed a hydrophilic behaviour and were easily infiltrated with aqueous solutions. Clean porous metal supports, however, were strongly hydrophobic and the wetting of aqueous solutions on them was not improved even when surfactants (TRITON, CTAB) were employed. However, positive results were obtained for mixtures containing organics with larger C fraction, for example, terpineol in conjunction with a dispersant, such as polyvinyl butyrate (PVB) (5 wt.%). While solutions of the Mn nitrate could not be made in terpineol, emulsions made of 50 vol % terpineol/PVB and 50 vol% ethanol-based solutions of the nitrates were found to be reasonably stable and would infiltrate well for the clean metal supports. A good compromise was

also found by using isopropanol which still provided sufficient wetting but also allowed the formation of clear nitrate solutions (Figure 4).

## 3.3 Composition and microstructure of the coatings

Figure 5 shows the XRD pattern and microstructure of a coated porous metal support with surface Si contamination. The XRD pattern confirms the presence of a spinel phase alongside the steel. No other reflections can be observed, suggesting perhaps that other unwanted phases, such as chromia or excess manganese oxide are not present (Figure 5 a). This is in good agreement with the calculated phase diagrams for Mn-Fe-Cr-$O_2$ system at 900 °C and $pO_2 \sim 10^{-20}$ atm and for Cr-Mn-$O_2$ system at 1000 °C for a wide range of $pO_2$ values, which show that the most probable phase to form for the given experimental conditions is a $(Mn,Cr)_3O_4$ spinel. Both surface and cross-section micrographs reveal that the coating is continuous over the surface of the steel grains, but some particles are also present, either on the coating or embedded in it, as shown in Figure 5 a, b. Close examination of the coating, as illustrated in Figure 5, seems to indicate that there is an apparent gap between the coating and the metal grains. However, EDX analysis carried on such regions, as illustrated in Figure 6, reveals that the apparent gap between the coating and the steel grains actually corresponds to Si and/or $SiO_2$. The Si-rich region appears dark, similar to the one occupied by the organic epoxy resin because the image was collected in backscattering mode, where contrast is based on relative atomic weight and density rather than morphology. Thus the brightness decreases in the order Steel>Spinel oxide>Si≈Resin, as seen in Figure 5. The elemental X-ray maps show the existence of oxygen and Mn in the coating layer, with Cr being well distributed in the FeCr particle and also in the coating. Fe is mostly present in the steel support, and to less extent in the coating layer, but there are also some indentations of Fe in the spinel coating, most likely corresponding to the particles observed on the surface as well. Overall, this probably indicates that

coating formed in this case consists of a $MnCr_2O_4$ or low Fe content $MnFe_xCr_{2-x}O_4$ spinel with occasional Fe islands (particles). The Si-rich interface layer between the spinel coating and the steel grains seems to contain a small amount of Fe and Cr, and a more considerable amount of Mn.

The presence of a Si-rich layer between the coating and the metal particles was confirmed by TEM and EDX, which also revealed that all these interfaces are continuous and there is no gap in between the coating and the substrate. The EDX data were collected for each zone indicated as 1 and 2 on the image presented in Figure 7 a and the EDX spectra presented in Figure 7 b shows the presence of Si in a Si-Mn layer (zone 1) and in the vicinity of the FeCr particle as a Si rich layer (zone 2). Figure 7 c indicates 4 different zones for which EDX spectra were collected and presented in Figure 7 d. Zone 1 contains Mn, Cr and a small amount of Si, which indicates both the formation of the spinel, but also another Si-Mn containing phase. Zone 2 indicates the presence of a Si layer, with the corresponding EDX spectra showing very small peaks of Fe and Cr, and a predominant peak corresponding to Si. Zone 3 and 4 correspond to the FeCr particle.

While the infiltration of water or ethanol-based nitrate solutions on surface Si-contaminated porous metal supports was easily achievable and straightforward, the use of similar solutions for infiltration of clean porous metal supports was much more challenging. This is because in the absence of Si surface contamination the metal surface became strongly hydrophobic and therefore aqueous or ethanol based solutions displayed very high wetting angles on the metal. In an attempt to improve the wetting, a small amount of cerium nitrate was infiltrated prior to the Mn nitrate solutions. However, a subsequent infiltration of Mn nitrate in ethanol did not show a significant improvement in comparison to the case where no ceria was used. Overall, the deposited layer was well distributed but not continuous as illustrated in Figure 8 a, b.

Better results were observed when terpineol-ethanol emulsions were employed for infiltration of the nitrate salts. Figure 8 c, d illustrates the results obtained on a cerium nitrate terpineol-ethanol emulsion infiltrated in a porous metal support, at percentage loading of ~5 wt.%.

The phases identified by means of XRD analysis are $CeO_2$ $CeCrO_3$ and $Cr_2O_3$, with rather small amount of perovskite phase (Figure 9), in agreement with the thermodynamic calculations.

Subsequent infiltration of ceria, followed by Mn:

The infiltration of Ce-nitrate (2 wt.%) in ethanol/terpineol emulsion followed by Mn-nitrate (1 wt.%) in ethanol/terpineol emulsion under vacuum, with intermediate calcinations resulted in an un-even distribution of Ce and Mn oxides. The initial $CeO_2$ coating inhibited the formation of $Cr_2O_3$ but also prohibited the formation of a MnCr spinel (the infiltrated Mn nitrate remained as MnO).

A substantial improvement in the infiltration process of Si-free porous metal supports, in terms of wetting, was accomplished when isopropanol based solutions in vacuum were used. Coatings appear to be uniform and continuous, especially on porous metal supports. However, unlike the case of Si-contaminated substrates, the composition of the coating is no longer composed exclusively of a spinel phase, but also of various amounts of chromia and manganese oxide. Moreover, these amounts seem to vary from sample to sample, possibly due to some substrate microstructure variation but possibly also reflecting the difficulty of achieving proper wetting consistently in these systems. Generally it was observed that half cells have a lower infiltrate uptake (~2-3 wt.%) as compared to the porous metal supports (~4-5 wt.%) which reflects in thinner coatings and more $Cr_2O_3$ for the former. XRD patterns collected on four different MS and MSHC infiltrated with Mn nitrate – isopropanol solution are compared in Figure 10, all showing the presence of $Cr_2O_3$ after coating, with inefficient scavenging effect of the infiltrated precursors as compared to Si-contaminated substrates. The micrographs of the coated MS and MSHC, included in Figure 11 and Figure 12, show that while the distribution and coverage of the coating layer in the porous metal

supports was relatively good, for half cells the metal particles in the support are unevenly coated. In particular, the metal particles in the critical anode functional layer display insufficient coating, although this could also be due to its relatively dense initial microstructure.

## 3.4 Corrosion resistance of coated substrates

Corrosion tests on spinel coated MS and spinel coated MSHC samples performed for 500 h at 850°C in an atmosphere consisting of $Ar/H_2O/H_2$ where $pH_2O/pH_2$=9 to simulated outlet anode gas at 90% fuel utilization are compared from post-oxidation cross-section micrographs. The high temperature was used to accelerate the corrosion process. In Figure 13 cross-section micrographs of the corroded spinel coated MS sample (a, b) and spinel coated MSHC sample (c, d) are compared to corroded non-coated MS sample (e, f) and Ni-CGO infiltrated/coated MSHC sample (g, h).

Corrosion tests on spinel coated MS and spinel coated MSHC samples were also performed for 500 h at 650°C in an atmosphere consisting of $Ar/H_2O/H_2$ where $pH_2O/pH_2$=9. The temperature corresponds to a realistic operation temperature for MS-SOFC. In Figure 14 cross-section micrographs of the corroded spinel coated MS sample (a, b) and spinel coated MSHC sample (c, d) are compared to corroded non-coated MS sample, exposed for 2000 h (e, f) and Ni-CGO infiltrated/coated MSHC sample (g, h).

The surface of the spinel coated MS sample consists of a non-continuous, poorly adherent oxide scale mixed with alloy chips seemingly separated from the bulk of the MS sample. The processing required for obtaining the spinel coating appears to have changed the corrosion behavior in comparison to an uncoated MS sample, since the oxide scale on the surface for the uncoated MS sample is thicker, continuous, and without any obvious separating alloy chips. Comparing the lower

magnifications in Figure 13(a) and (e) it would appear as if the surfaces in the pores in the spinel coated samples are more corroded (pores are clogged) than the surfaces in the pores of the uncoated MS sample (more open pores), although the initial porosity was higher in the latter, making a direct comparison difficult. However, the observed relatively thick continuous oxide scale on the uncoated MS samples probably blocked gas access through the pores on the surface restricting the degree of corrosion within the metal body.

A similar oxide scale structure is observed on the spinel coated MS sample as was observed on the surface of the spinel coated MSHC sample. The MS structure of the Ni-CGO coated MSHC sample is however equipped with a significantly thinner oxide after 500 h corrosion at 850°C, although the initial thickness of the coating was also smaller, which could affect the final results. As illustrated in Figure 13 for the spinel and Ni-CGO coated MSHC samples in (c, d) and (g, h) respectively the metal phase in the ScYSZ/FeCr cermet anode functional layer is severely corroded with obvious break-away oxidation as a result. This is causing the ScYSZ electrolyte to break off. The coatings were clearly not efficient enough at protecting the metal surfaces at this temperature in the ScYSC/FeCr-cermet. However the surface area of the metal phase versus its bulk in the ScYSC/FeCr-cermet layer is also high making it extremely vulnerable, as also found by Molin et al.[25] The break-away oxidation observed for the pre-oxidized MS and MSHC may be associated with the decrease of Cr concentration in the metal particles.[26,27]

As expected the degree of corrosion rate was less at 650°C, (Figure 14). Both the spinel (exposed 500 h) and the uncoated MS (exposed for 2000 h) samples have a few restricted areas where more extensive oxidation has taken place. They do however not seem to be spreading out of control. Disregarding these heavily oxidized areas and studying the surface of the spinel coated MS sample in Figure 14 (a, b) the oxide scale is non-continuous, with numerous alloy “chips” reminiscent of the corresponding sample corroded at 850 °C in Figure 13 (a, b). The oxide scales inside the pores of the spinel coated MS sample seem thicker and more continuous than the oxide scale on the surface. The

oxide scales on the surface and inside the pores of the uncoated MS sample in Figure 14 (e, f) exposed for 2000 h are in general presenting a thin, continuous appearance if the few heavily oxidized areas are disregarded. This illustrates the key role played by the starting microstructure, morphology and surface characteristics of the MS or MSHC in achieving effective corrosion resistance. These characteristics appear to affect not only the initial quality of the produced coating but also subsequent oxidation behavior.

The oxide scales in the MS structure of the Ni-CGO coated MSHC sample in Figure 14 (g, h) are difficult to discern with the resolution of the used microscope used to collect the micrographs in Figure 13 and Figure 14. On the metal phase in the ScYSZ/FeCr-cermet layer a continuous oxide scale is clear to observe though (enhanced by the bright contrast of the surrounding ScYSZ) as well as areas with the beginnings of heavy oxidation. The pre-oxidation of the metal particles for chromia scale formation, and the repeated low temperature oxidation treatments, during infiltration of Mn nitrate solution were detrimental to the final oxidation resistance, after obtaining the spinel layer inside the metal supports. The spinel coating did not seem to be efficient enough to hinder break away oxidation of the entire metal phase in the ScYSZ/FeCr-cermet layer.

# 4 Conclusions

Continuous and relatively thin (<1 µm) coatings were successfully prepared on porous metal scaffolds by scavenging a thin oxide chromia layer into MnFeCr based spinels by using Mn nitrate solutions. The quality of the coating and means to produce it was found to strongly depend on the quality of the surface of the metal supports. The surface of clean metal supports was highly hydrophobic and as such isopropanol based Mn nitrate solutions were used successfully to produce coatings on such surface. Metal surfaces with trace contamination of silicon oxide were hydrophilic

and thus aqueous solutions could be used for infiltration in this case. However, in this case, a silicon-rich layer would persist between the metal and the coating.

The corrosion resistance tests suggest that the effectiveness of coatings is dictated not only by the composition and structure of the coatings but also by the microstructure and surface characteristics of the metal scaffolds because the latter affect the quality of the initial coating and subsequent oxidation behaviour.

Acknowledgements

The authors thank European Union's Seventh Framework Programme (FP7/2007-2013) for Fuel Cell and Hydrogen Joint Technology initiative under grant agreement no. [FCH JU-GA 278257]10 for financial support.

# 5 References

[1] T. Klemensø, J. Nielsen, P. Blennow, Å.H. Persson, T. Stegk, B.H. Christensen, S. Sønderby, High performance metal-supported solid oxide fuel cells with Gd-doped ceria barrier layers, J. Power Sources. 196 (2011) 9459–9466. doi:10.1016/j.jpowsour.2011.07.014.

[2] J. Nielsen, T. Klemensø, P. Blennow, Detailed impedance characterization of a well performing and durable Ni:CGO infiltrated cermet anode for metal-supported solid oxide fuel cells, J. Power Sources. 219 (2012) 305–316. doi:10.1016/j.jpowsour.2012.07.031.

[3] P. Blennow, J. Hjelm, T. Klemensø, A. Persson, K. Brodersen, A. Srivastava, H. Frandsen, M. Lundberg, S. Ramousse, M. Mogensen, Development of Planar Metal Supported SOFC with Novel Cermet Anode, ECS Trans. 25 (2009) 701–710. doi:10.1149/1.3205585.

[4] P. Blennow, J. Hjelm, T. Klemensø, S. Ramousse, A. Kromp, A. Leonide, A. Weber, Manufacturing and characterization of metal-supported solid oxide fuel cells, J. Power Sources. 196 (2011) 7117–7125. doi:10.1016/j.jpowsour.2010.08.088.

[5] A. Kromp, J. Nielsen, P. Blennow, T. Klemensø, A. Weber, Break-down of Losses in High Performing Metal-Supported Solid Oxide Fuel Cells, Fuel Cells. 13 (2013) 598–604. doi:10.1002/fuce.201200165.

[6] M.C. Tucker, Progress in metal-supported solid oxide fuel cells: A review, J. Power Sources. 195 (2010) 4570–4582. doi:10.1016/j.jpowsour.2010.02.035.

[7] P. Blennow, B.R. Sudireddy, Å.H. Persson, J. Nielsen, R.N. Sachitanand, J. Froitzheim, Investigation of Cu-Based Infiltration Coatings for Metal-Supported SOFC, ECS Trans. 57 (2013) 771–780. doi:10.1149/05701.0771ecst.
[8] S. Molin, M. Chen, P.V. Hendriksen, Oxidation study of coated Crofer 22 APU steel in dry oxygen, J. Power Sources. 251 (2014) 488–495. doi:10.1016/j.jpowsour.2013.09.100.
[9] V. Venkatachalam, S. Molin, M. Chen, I. Smirnov, P.-O. Larsson, P.V. Hendriksen, N. Bonanos, Optimization of ferritic steel porous supports for protonic fuel cells working at 600°C, Mater. Sci. Technol. 2014 Conf. ASM International (2014) 1231–1240. doi:10.13140/2.1.4342.7845.
[10] S. Molin, M. Gazda, P. Jasinski, Coatings for improvement of high temperature corrosion resistance of porous alloys, J. Eur. Ceram. Soc. 31 (2011) 2707–2710. doi:10.1016/j.jeurceramsoc.2011.02.007.
[11] M. Stange, C. Denonville, Y. Larring, C. Haavik, A. Brevet, A. Montani, O. Sicardy, J. Mougin, P.-O. Larsson, Coating Developments for Metal-Supported Solid Oxide Fuel Cells, ECS Trans. 57 (2013) 511–520. doi:10.1149/05701.0511ecst.
[12] A. Magrasó, H. Falk-Windisch, J. Froitzheim, J.-E. Svensson, R. Haugsrud, Reduced long term electrical resistance in Ce/Co-coated ferritic stainless steel for solid oxide fuel cell metallic interconnects, Int. J. Hydrog. Energy. (n.d.). doi:10.1016/j.ijhydene.2015.04.147.
[13] P. Blennow, B.R. Sudireddy, Å.H. Persson, T. Klemensø, J. Nielsen, K. Thydén, Infiltrated SrTiO3:FeCr-based Anodes for Metal-Supported SOFC, Fuel Cells. 13 (2013) 494–505. doi:10.1002/fuce.201200176.
[14] R. Knibbe, H.-J. Wang, P. Blennow, K. Thydén, Å.H. Persson, L. Mikkelsen, T. Klemensø, Oxidation in ceria infiltrated metal supported SOFCs – A TEM investigation, J. Power Sources. 228 (2013) 75–82. doi:10.1016/j.jpowsour.2012.11.051.
[15] A. Petric, H. Ling, Electrical Conductivity and Thermal Expansion of Spinels at Elevated Temperatures, J. Am. Ceram. Soc. 90 (2007) 1515–1520. doi:10.1111/j.1551-2916.2007.01522.x.
[16] X. Chen, P. Hou, C. Jacobson, S. Visco, L. Dejonghe, Protective coating on stainless steel interconnect for SOFCs: oxidation kinetics and electrical properties, Solid State Ion. 176 (2005) 425–433. doi:10.1016/j.ssi.2004.10.004.
[17] Z. Yang, G.-G. Xia, C.-M. Wang, Z. Nie, J. Templeton, J.W. Stevenson, P. Singh, Investigation of iron–chromium–niobium–titanium ferritic stainless steel for solid oxide fuel cell interconnect applications, J. Power Sources. 183 (2008) 660–667. doi:10.1016/j.jpowsour.2008.05.037.
[18] Z. Yang, G. Xia, X. Li, J. Stevenson, (Mn,Co)3O4 spinel coatings on ferritic stainless steels for SOFC interconnect applications, Int. J. Hydrog. Energy. 32 (2007) 3648–3654. doi:10.1016/j.ijhydene.2006.08.048.
[19] E. Stefan, J.T.S. Irvine, Synthesis and characterization of chromium spinels as potential electrode support materials for intermediate temperature solid oxide fuel cells, J. Mater. Sci. 46 (2011) 7191–7197. doi:10.1007/s10853-010-4489-1.
[20] E. Stefan, P.A. Connor, J.T.S. Irvine, Development and performance of MgFeCrO4 – based electrodes for solid oxide fuel cells, J. Mater. Chem. A. 1 (2013) 8262. doi:10.1039/c3ta11496a.
[21] E. Stefan, G. Tsekouras, J.T.S. Irvine, Development and Performance of MnFeCrO4-based Electrodes for Solid Oxide Fuel Cells, Adv. Energy Mater. 3 (2013) 1454–1462. doi:10.1002/aenm.201300361.
[22] E. Stefan, P.A. Connor, A.K. Azad, J.T.S. Irvine, Structure and properties of MgMxCr2−xO4 (M = Li, Mg, Ti, Fe, Cu, Ga) spinels for electrode supports in solid oxide fuel cells, J. Mater. Chem. A. (2014). doi:10.1039/C4TA03633F.
[23] C.W. Bale, P. Chartrand, S.A. Degterov, G. Eriksson, K. Hack, R. Ben Mahfoud, J. Melançon, A.D. Pelton, S. Petersen, FactSage thermochemical software and databases, Calphad. 26 (2002) 189–228. doi:10.1016/S0364-5916(02)00035-4.
[24] C.W. Bale, E. Bélisle, P. Chartrand, S.A. Decterov, G. Eriksson, K. Hack, I.-H. Jung, Y.-B. Kang, J. Melançon, A.D. Pelton, C. Robelin, S. Petersen, FactSage thermochemical software and

databases — recent developments, Calphad. 33 (2009) 295–311. doi:10.1016/j.calphad.2008.09.009.

[25] S. Molin, M. Gazda, P. Jasinski, High temperature oxidation of porous alloys for solid oxide fuel cell applications, Solid State Ion. 181 (2010) 1214–1220. doi:10.1016/j.ssi.2010.06.049.

[26] L. Singheiser, P. Huczkowski, T. Markus, W.J. Quadakkers, High Temperature Corrosion Issues for Metallic Materials in Solid Oxide Fuel Cells, in: Shreirs Corros., Elsevier, 2010: pp. 482–517. http://linkinghub.elsevier.com/retrieve/pii/B978044452787500024X (accessed November 7, 2016).

[27] P. Huczkowski, V. Shemet, J. Piron-Abellan, L. Singheiser, W.J. Quadakkers, N. Christiansen, Oxidation limited life times of chromia forming ferritic steels, Mater. Corros. 55 (2004) 825–830. doi:10.1002/maco.200303798.

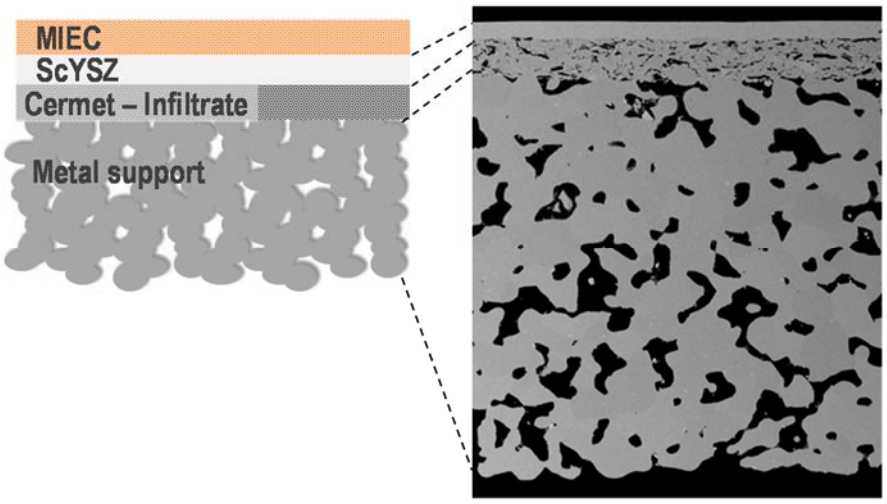


**Figure 1 Schematic illustration showing the concept of the metal supported cell design.**

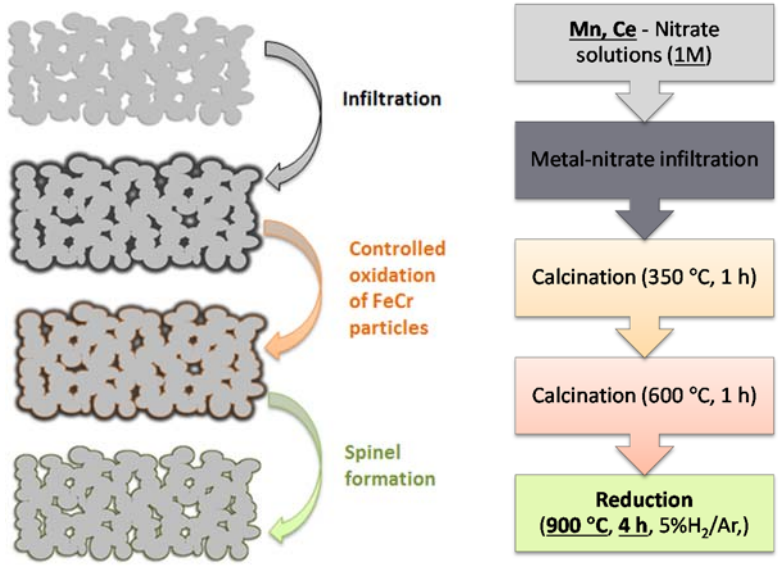


**Figure 2 Schematic representation of infiltration process and intermediate thermal treatments applied; Calcinations at 350 °C and 600 °C, in air.**

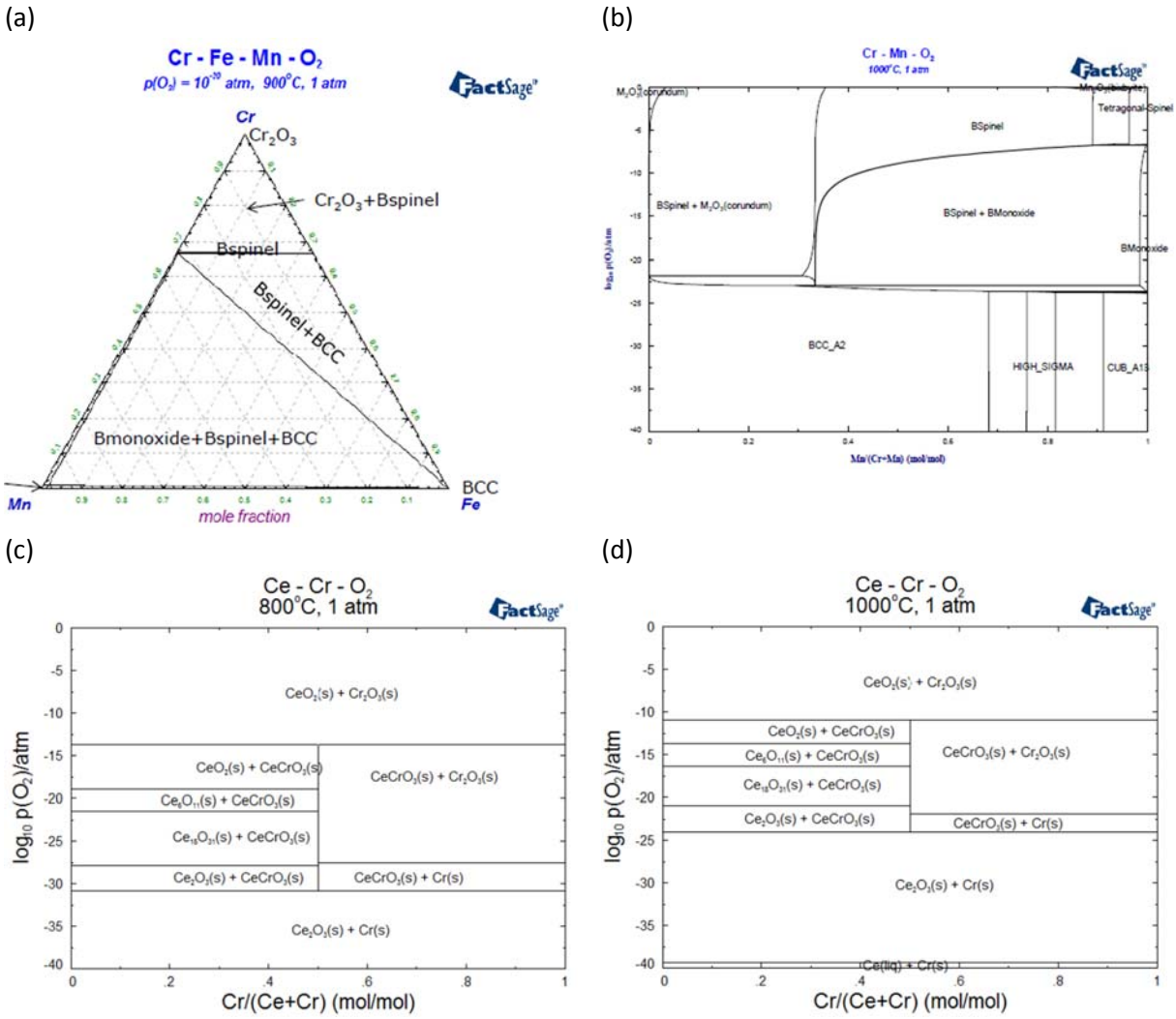


**Figure 3 Calculated phase diagrams of oxide systems under low $pO_2$ conditions for in-situ coating of metal supports for SOFC application.**

| | |
|---|---|
| 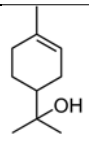 | Terpineol – slightly too viscous and hydrophobic even as emulsion |
|  | Isopropanol – appropriate viscosity, wetting and nitrate solubility |

**Figure 4 Graphic representations of the solvents which demonstrated better results in terms of wetting the metal surface.**

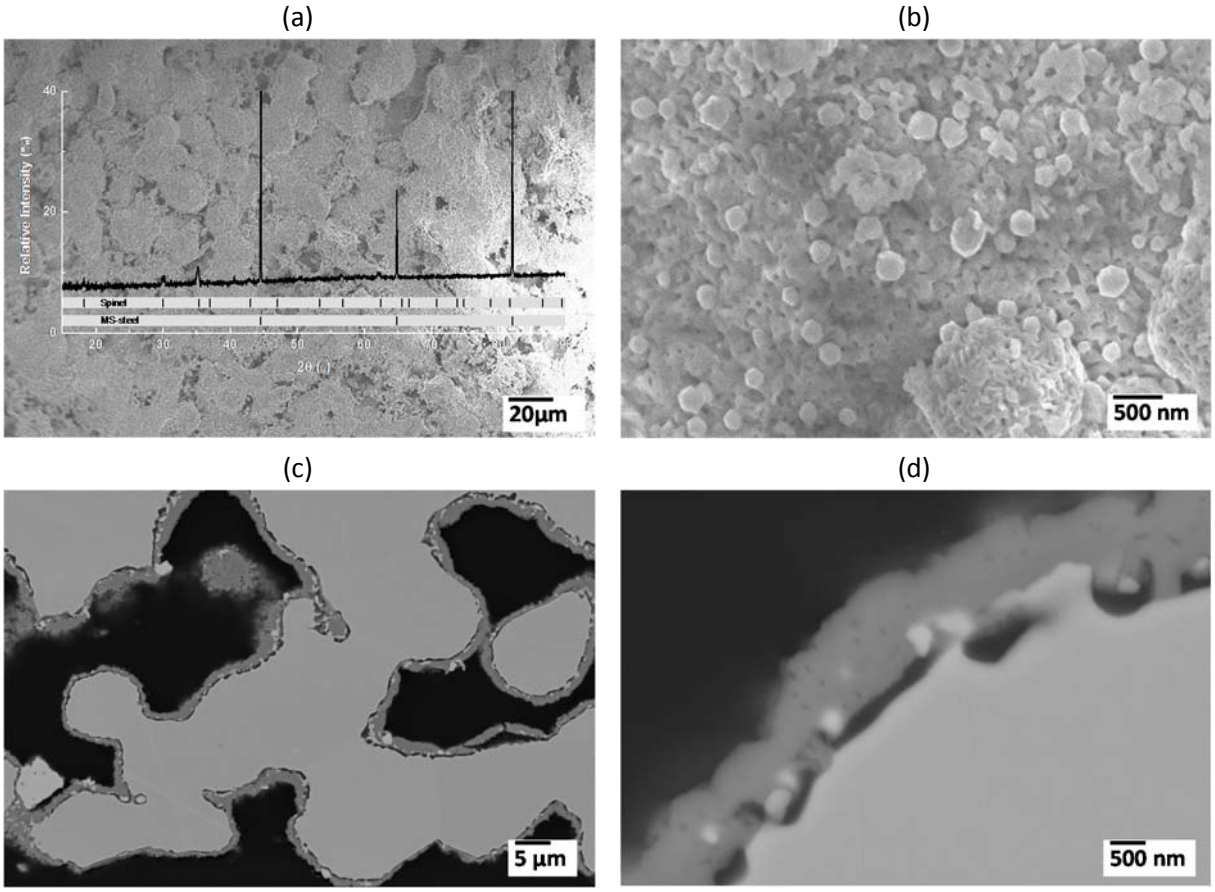


**Figure 5 Mn infiltrated in a 1 % 3YSZ-MS : (a) and (b) – Surface micrograph; (c) and (d) – Cross section micrographs of the sample after the final thermal treatment at 900 °C for 4 hours in 5%$H_2$/Ar.**

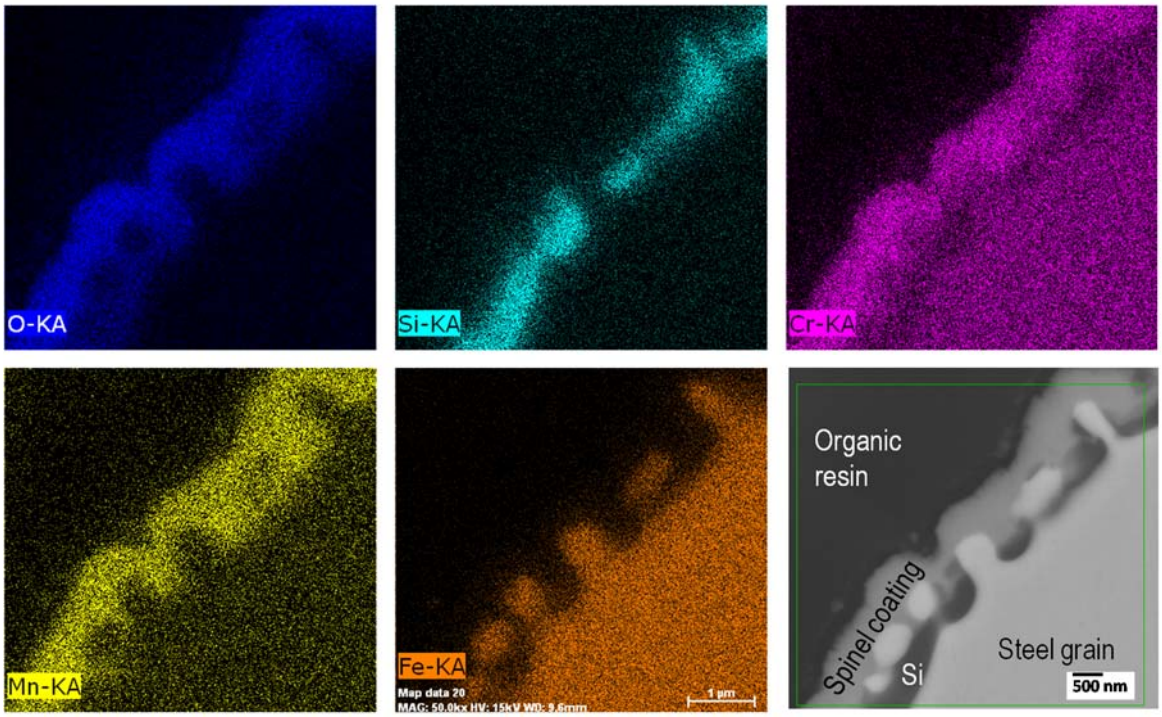


**Figure 6 EDX maps collected at the interface spinel/MS for a Mn-infiltrated 1 % 3YSZ-MS.**

(a)

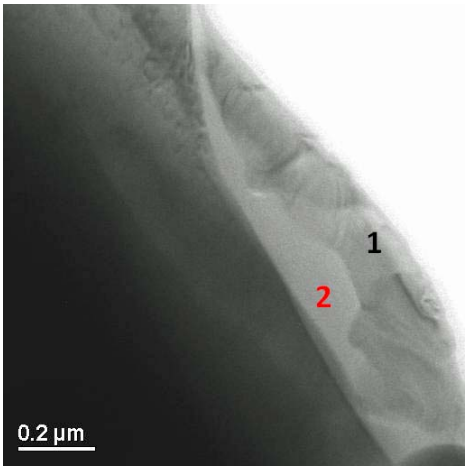


(b)

(c)

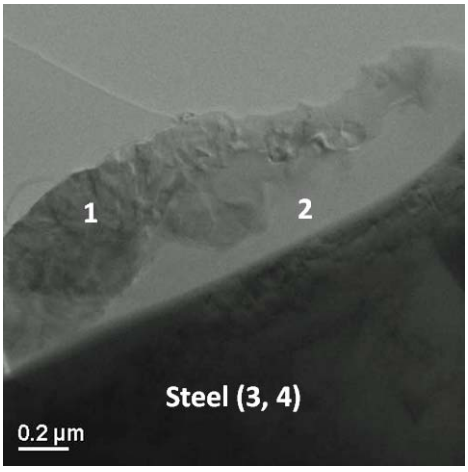


(d)

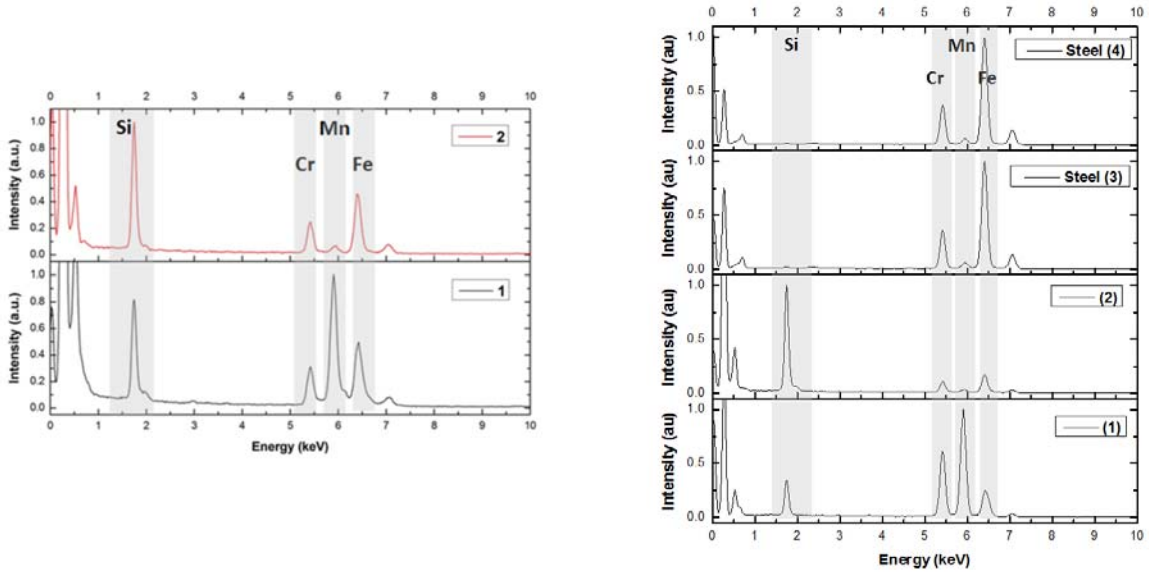


**Figure 7 Transmission electron microscopy and EDX analysis on the spinel coated MS, showing the existence of a thin layer of Si at the interface spinel/MS.**

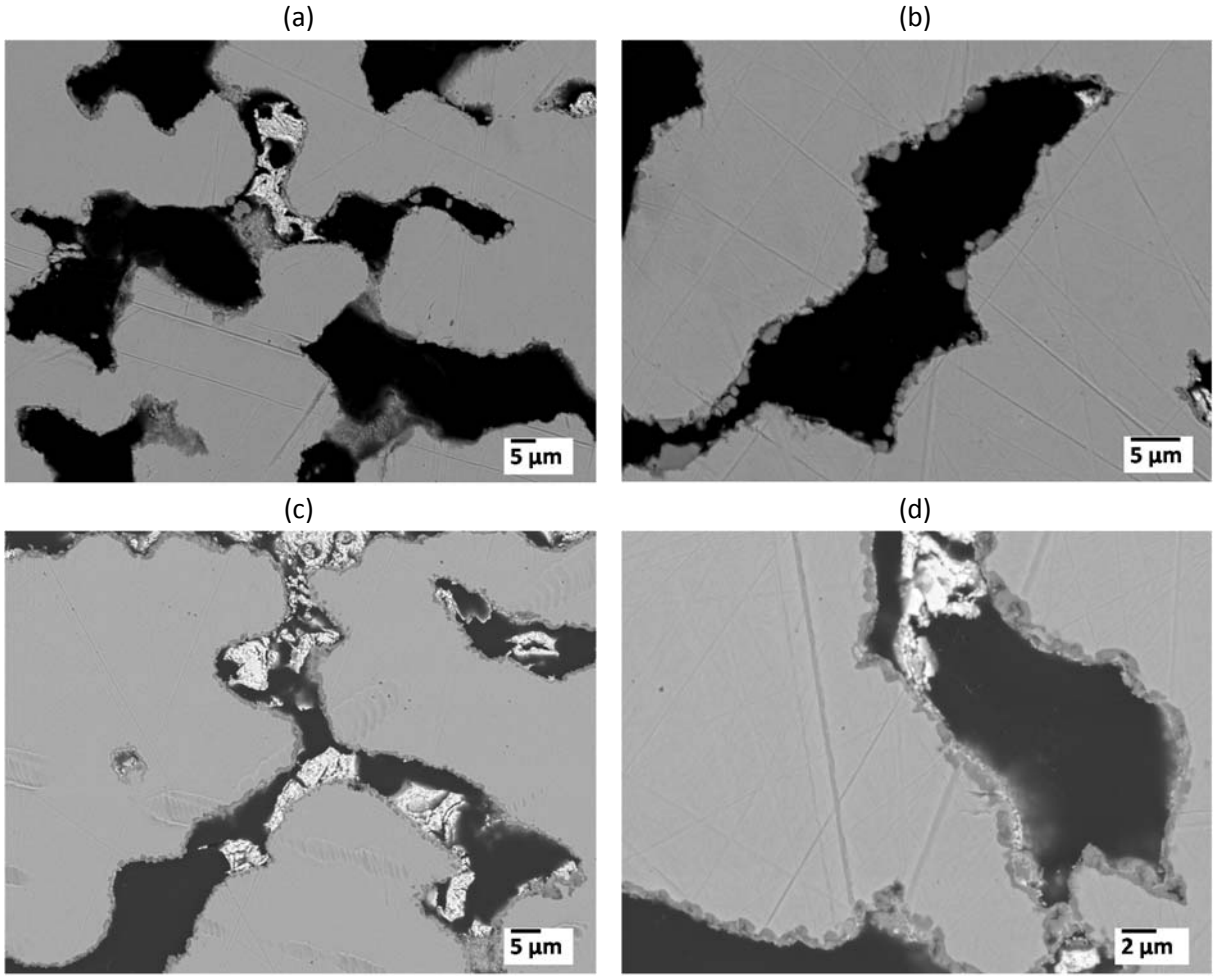


**Figure 8. Cross-sectional micrographs of MS infiltrated with: (a) and (b) $CeO_2$ followed by Mn nitrate in ethanol solution; (c) and (d) $CeO_2$ as emulsion of the ethanol nitrate solution with terpineol/PVB, infiltrated under vacuum on MS.**

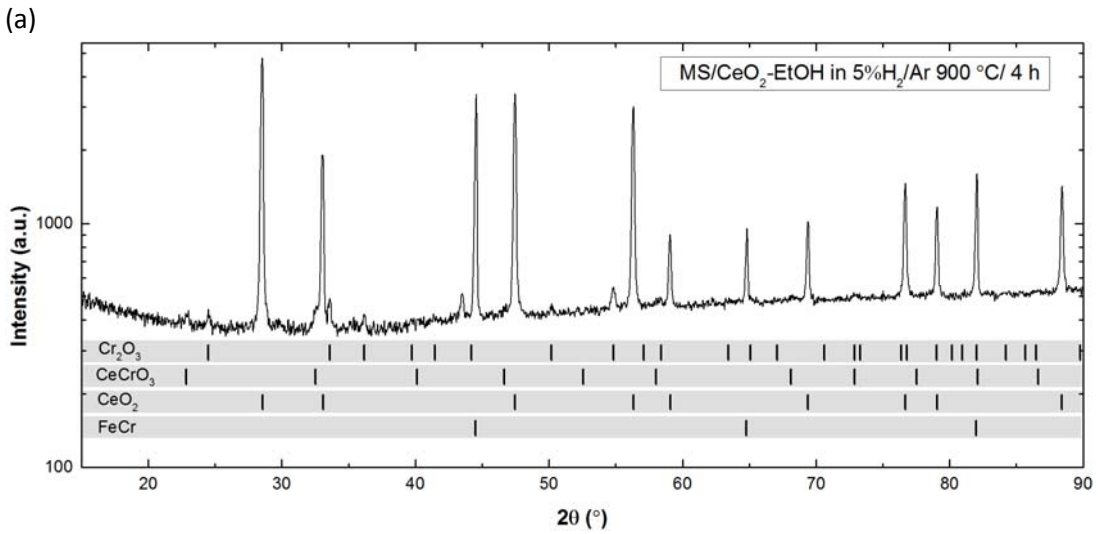

(b)

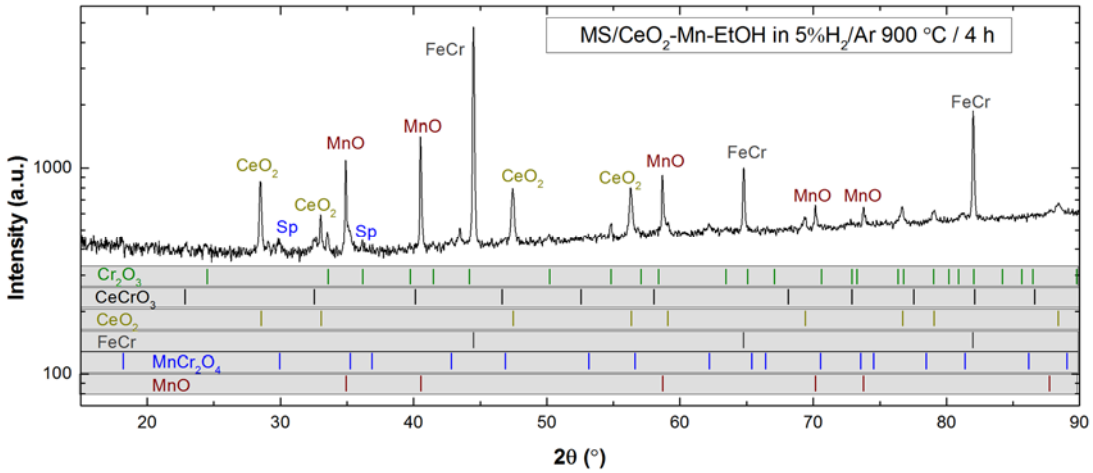


**Figure 9. X-ray diffraction patterns collected on MS after: (a) infiltration with ceria as emulsion ethanol/terpineol (PVB), under vacuum (b) sequential infiltration with ceria and Mn oxide as emulsions ethanol/terpineol (PVB), under vacuum.**

(a)

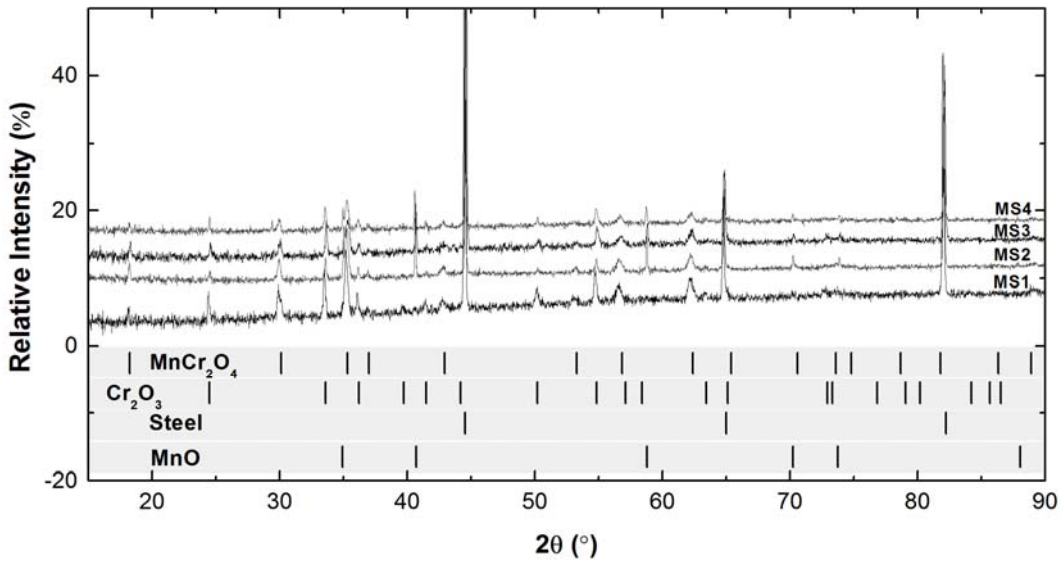


(b)

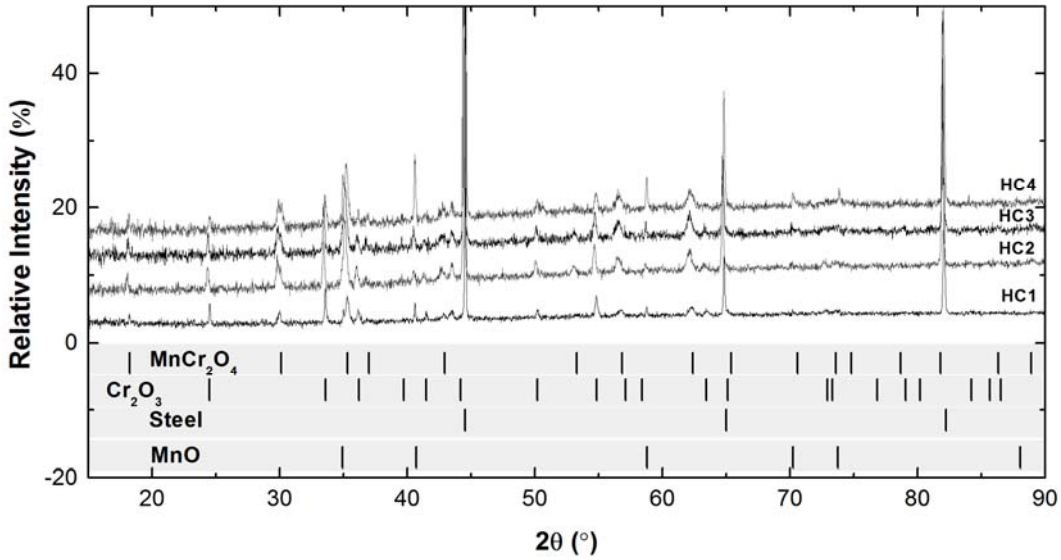


Figure 10. X-ray diffraction patterns collected after infiltration with Mn nitrate – IPA solution, under vacuum and subsequent thermal treatments on (a) MS and (b) MSHC.

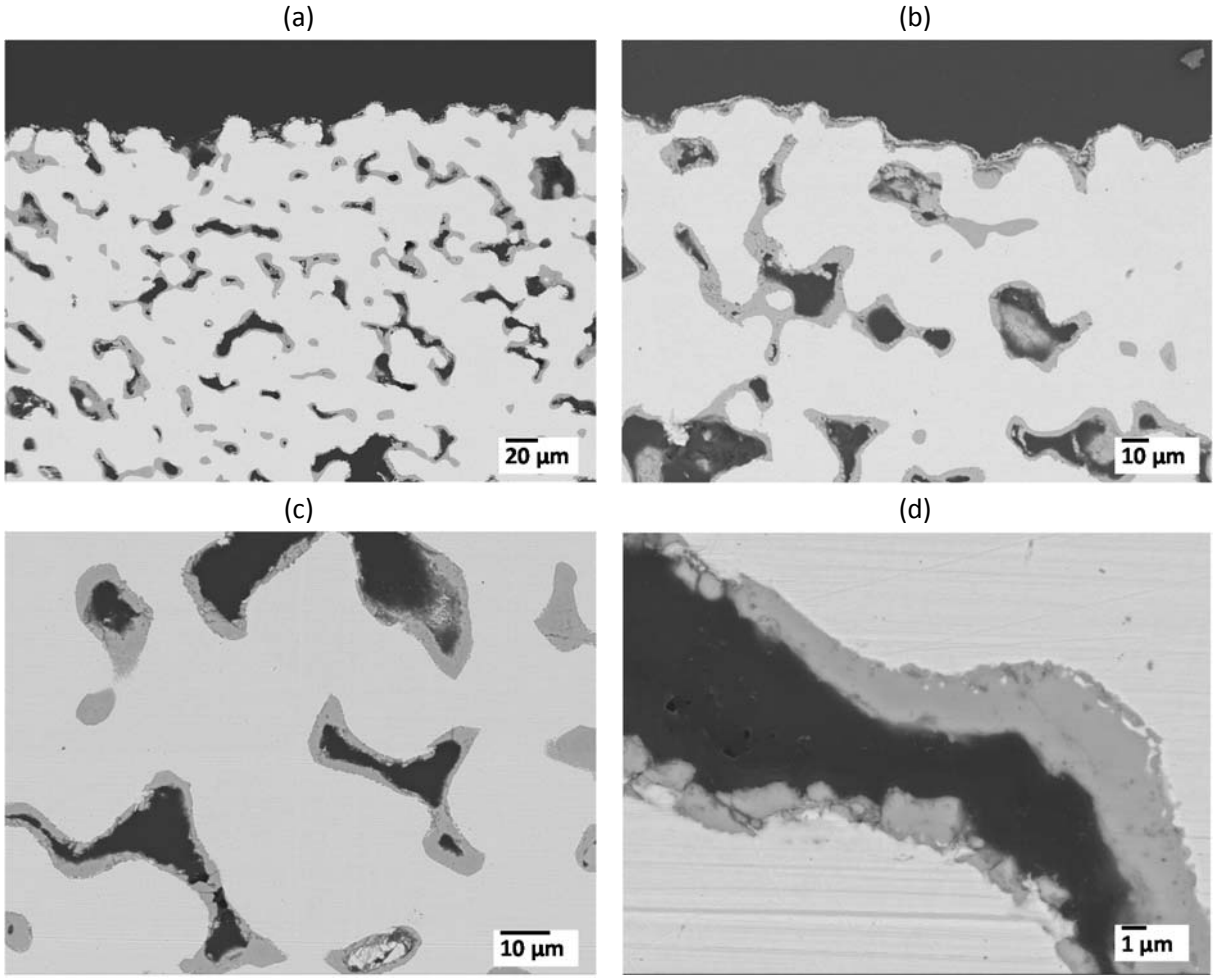


**Figure 11.Cross-sectional micrographs of MS after infiltration with Mn nitrate – IPA solution, under vacuum and subsequent thermal treatments.**

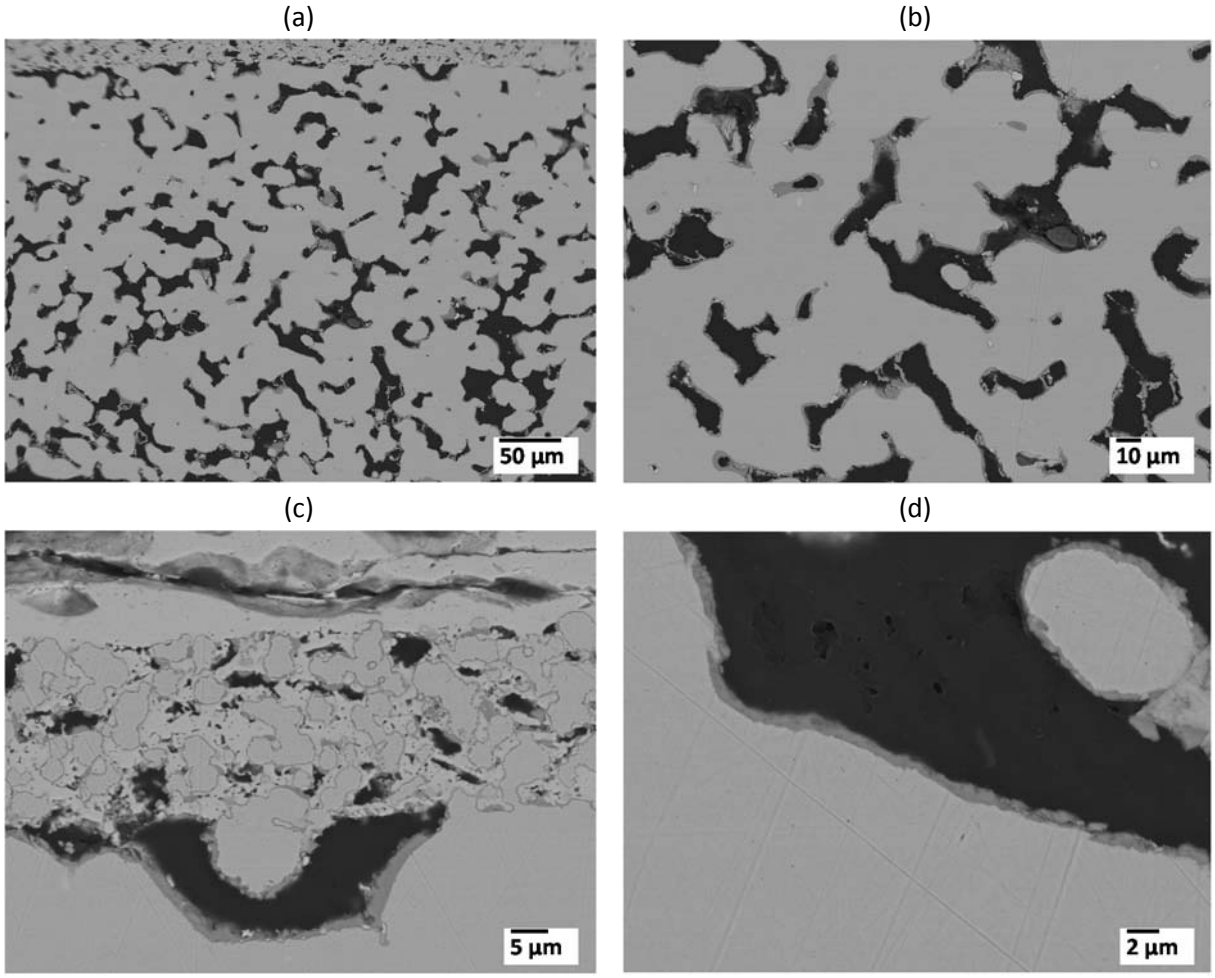


**Figure 12 Cross-sectional micrographs of MSHC after infiltration with Mn nitrate – IPA solution, under vacuum and subsequent thermal treatments.**

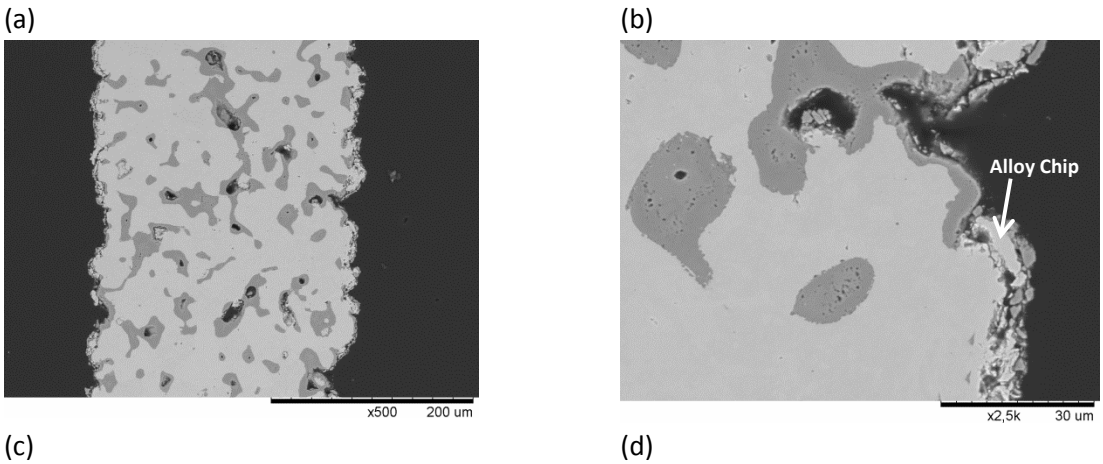

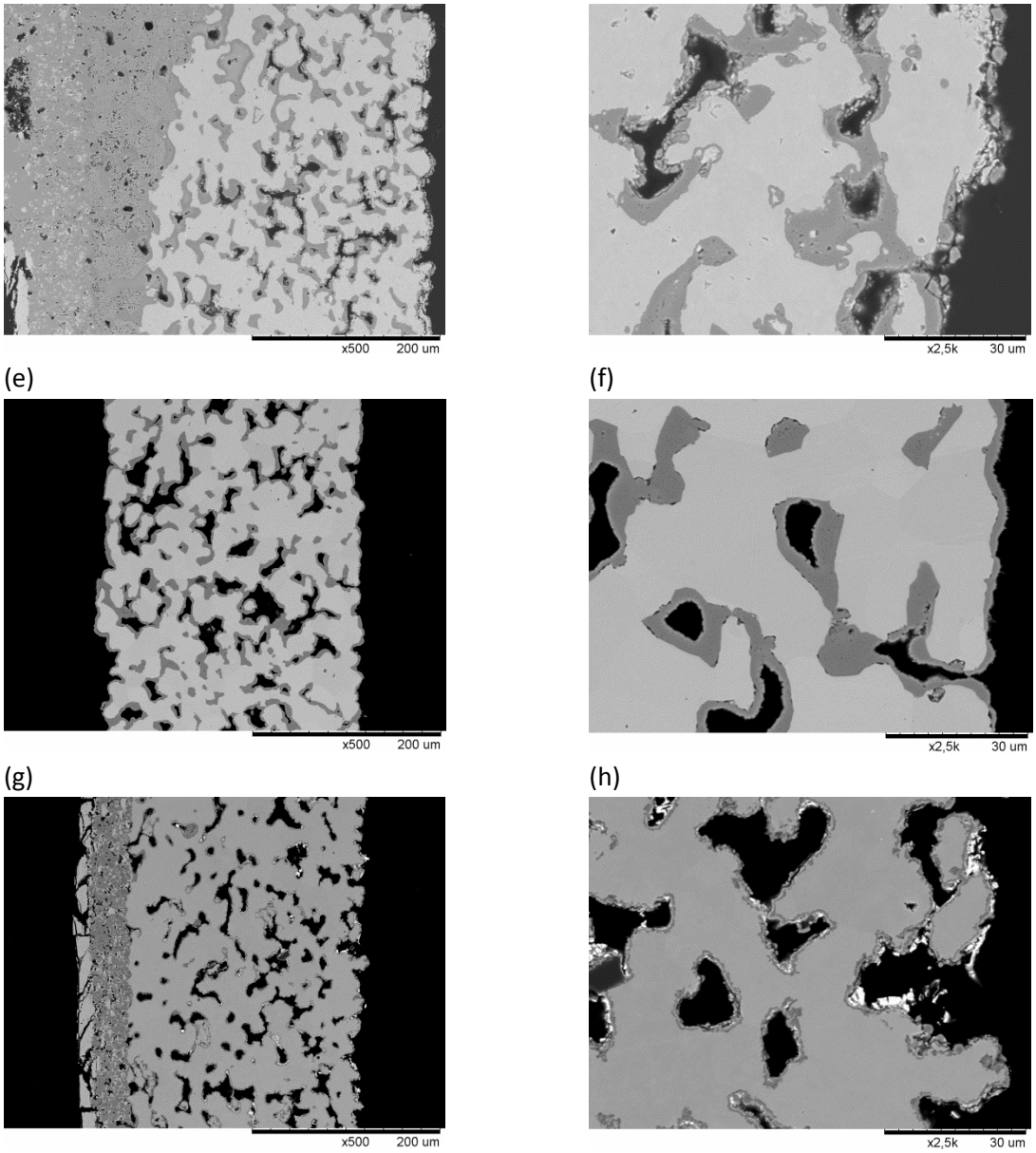


**Figure 13. Cross-sections of (a,b) spinel coated MS sample, (c,d) spinel coated MSHC sample, (e,f) uncoated MS sample and (g,h) Ni-CGO infiltrated MSHC sample corroded at 850°C for 500 h in an atmosphere consisting of $Ar/H_2O/H_2$ where $pH_2O/pH_2$=9 to simulate anode outlet gas with 90% fuel utilization.**

(a) (b)

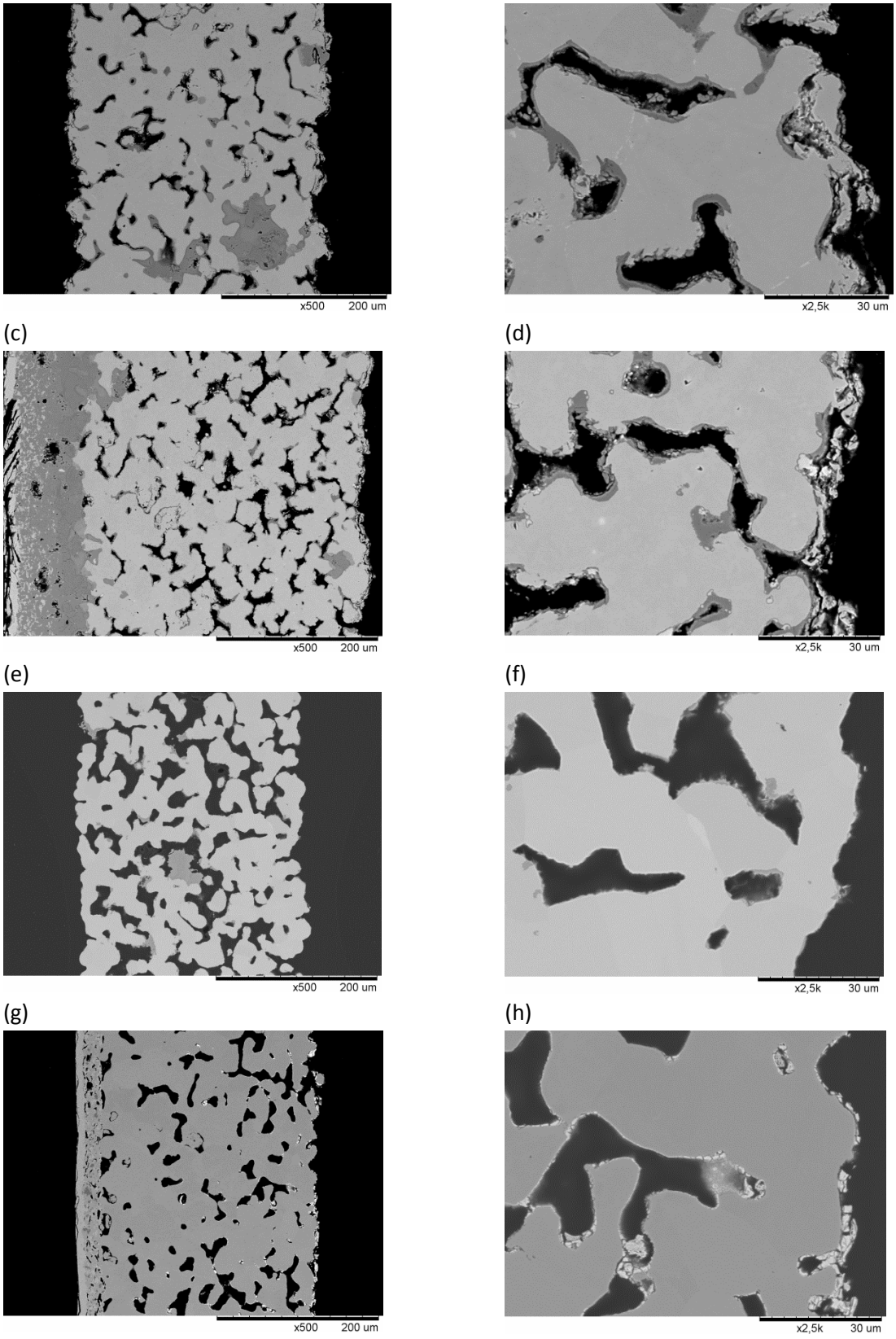


**Figure 14. Cross-sections of (a,b) spinel coated MS sample, (c,d) spinel coated MSHC sample, (e,f) uncoated MS sample and (g,h) Ni-CGO infiltrated/coated MSHC sample corroded at 650°C for 500 h in an atmosphere consisting of $Ar/H_2O/H_2$ where $pH_2O/pH_2$=9 to simulate anode outlet gas with 90% fuel utilization, except the uncoated MS sample that was corroded for 2000 h.**